

Alma Mater Studiorum Università di Bologna  
Archivio istituzionale della ricerca

On the importance of detailed structure in molecular electronics (and why microscopic models cannot see the wood for trees)

This is the final peer-reviewed author's accepted manuscript (postprint) of the following publication:

*Published Version:*

Thompson, I.R., Coe, M.K., Walker, A.B., Ricci, M., Roscioni, O.M., Zannoni, C. (2018). On the importance of detailed structure in molecular electronics (and why microscopic models cannot see the wood for trees). LIQUID CRYSTALS, 45(13-15, SI), 2086-2096 [10.1080/02678292.2018.1512666].

*Availability:*

This version is available at: <https://hdl.handle.net/11585/668098> since: 2019-02-19

*Published:*

DOI: <http://doi.org/10.1080/02678292.2018.1512666>

*Terms of use:*

Some rights reserved. The terms and conditions for the reuse of this version of the manuscript are specified in the publishing policy. For all terms of use and more information see the publisher's website.

This item was downloaded from IRIS Università di Bologna (<https://cris.unibo.it/>).  
When citing, please refer to the published version.

(Article begins on next page)

## **On the importance of detailed structure in molecular electronics (and why microscopic models cannot see the wood for trees)**

**Ian R Thompson, Mary K Coe, Alison B Walker, Matteo Ricci, Otello M Roscioni & Claudio Zannoni**

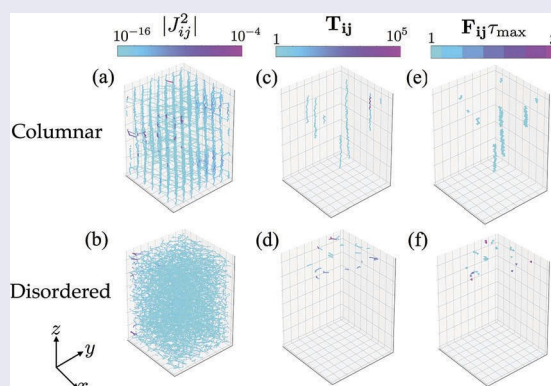
# On the importance of detailed structure in molecular electronics (and why microscopic models cannot see the wood for trees)

Ian R Thompson<sup>a</sup>, Mary K Coe<sup>a</sup>, Alison B Walker<sup>a</sup>, Matteo Ricci<sup>b</sup>, Otello M Roscioni<sup>b</sup> and Claudio Zannoni<sup>b</sup>

<sup>a</sup>Department of Physics, University of Bath, Bath, United Kingdom; <sup>b</sup>Dipartimento di Chimica Industriale 'Toso Montanari' and INSTM, Università di Bologna, Bologna, Italy

## ABSTRACT

We study the charge transport properties of a system of liquid crystalline molecules in two distinct phases. To differentiate between the two phases, we use a self-consistent model that describes the pairwise interaction between molecules, the electronic coupling between them and the difference in orbital energies. This multi-scale approach hinges upon having systems that are both accurate (to within atomic resolution) and large ( $\sim 10,000$  molecules). The two phases have dramatically different charge transport network topologies directly correlated to their molecular structures. We quantify the charge transport on both a macroscopic and microscopic scale, taking advantage of the model's resolution to understand the role of molecular packing in charge transport.



## 1. Introduction

Organic electronics are a rapidly advancing technology and promise many advantages over traditional silicon semiconductors. Aside from being recyclable, lightweight, flexible and easy to produce [1], the range of candidate organic molecules, and combinations thereof, means that organic electronics are in principle, extremely tunable. As an obvious corollary to this is that if there are many possible molecules, and the structure of a molecule affects its electronic properties, then finding the 'best' molecules is a difficult task. Thus computational screening of candidate molecules is a critical requirement for designing organic electronic devices [2]. Multi-scale modelling of a candidate organic semiconductor (OSC) must begin with a consideration of a single molecule and end with a description of the electrical properties of a bulk sample.

Charge conduction in organic systems occurs through a very different mechanism from conventional metallic/crystalline conductors and semiconductors. The transport occurs through a series of discrete charge carrier hops between localised sites, rather than through normal band transport [3,4]. As such, charge transport cannot be considered in reciprocal space and the local real space environment around the mechanism is crucial [5]. The probability of transition between two molecules is proportional to the overlap of their electronic orbitals so, broadly speaking, one would expect an exponential reduction in the hopping rate as molecules move apart. The key charge transport parameters are primarily influenced by the local orientation, structure and position of the molecules [6] – without an accurate structure one is forced to assume a prior value or distribution.

**Figure 1.**(Colour online) A schematic showing the atomic structure of HOTT and the equivalent coarse-grained bead that replaces the molecule (top)and small sections of the many-body morphologies (bottom).

between a hexagonally packed columnar phase and an isotropic phase [9,10]. By self-consistently modelling the rings of the molecule. From the atomic structure we know the positions and, crucially, the orientations of charge transport properties of the two phases we will demonstrate our multi-scale methodology and distinguish these sections relative to one another. We calculated distinct electronic regimes that a lattice model could not.

The development and application of CGMD is a non-trivial task. To effectively capture the interactions of multiple, overlapping atomic potentials with a single, effective two body potential is a challenge few appreciate.

One cannot implement too many parameters or degrees of freedom, lest the interaction become too complex and negate any numerical speed up; however, it cannot be too coarse an approximation lest it create false degeneracies in the potential landscape. A coarse-grained model of HOTT has been previously developed that recreates the columnar to isotropic phase transition [8].

$$k_{ij} = \frac{|J_{ij}|^2}{h} \frac{\pi}{\lambda k_B T} \exp \left( -\frac{\Delta G_j}{4\lambda k_B T} \right) \quad (2)$$

where  $J$  is the electronic transfer integral between sites,  $\lambda$  is the reorganisation energy of the system during the charge transfer process,  $\Delta G_j$  is the change in the Gibbs free energy before and after the process,  $k_B$  is Boltzmann's constant and  $T$  is the temperature. The change in the Gibbs energy is calculated in electron volts as

$$\Delta G_j = \frac{q}{j} \left( E_j - \phi_j \right) \quad (3)$$

## 2. Method

To simulate the dynamics of HOTT, Zannoni and coworkers used a Gay-Berne potential [11] that has both an angular and a separation dependence:

$$U(\hat{u}_i, \hat{u}_j; \hat{r}_{ij}) = \frac{\sigma_0}{r_{ij}^6} \left( 1 - \frac{1}{2} \left( \frac{\hat{u}_i \cdot \hat{u}_j}{|\hat{u}_i| |\hat{u}_j|} \right)^2 \right) \quad (1)$$

where  $\hat{u}_i$  is the unit vector that describes the orientation of molecule  $i$ ,  $\sigma_0$  fixes the scales of length (energy), while  $\hat{u}_i \cdot \hat{u}_j$  and  $\hat{r}_{ij}$  correspond to the anisotropic contact distance and potential well depth, respectively.

Determining the precise expressions for  $\sigma$  and  $\sigma_0$  are critical to reproducing the correct potential. This was performed by ProZannoni's group; if the reader wants more information, we would refer them to [9]. For this study it suffices that their model allowed large systems (10,000 molecules) to be equilibrated in two structural phases at two temperatures: an amorphous, isotropic phase at 400 K and an ordered phase of hexagonally packed columns at 280 K. Finally, they were able to map the positions of individual atoms back onto the coarse-grained molecular coordinates, resulting in an atomically resolved equilibrium structure. Figure 1 shows the atomic structure of HOTT, the size and shape of the coarse-grained bead used in the MD simulations and the resultant back mapping that can be performed.

We can use the equilibrated structure as the system that charge transport occurs throughout. Charge carriers can hop between sites of localised charge density

where  $q$  is the charge of the particle performing the hop,  $E$  is the site energy (equivalent to the HOMO energy for holes and the LUMO energy for electrons) and  $\phi$  is the electrostatic potential at the hopping site position. In a departure from standard practice, we solve the discretised Poisson's equation with a cloud-in-cell method to allow for the long range nature of the Coulomb interactions [13],

$$\nabla^2 \phi = \frac{\rho}{\epsilon_0} \quad (4)$$

where  $\phi$  is the discretised electric potential and  $\epsilon_0$  is the permittivity of free space multiplied by the material's dielectric constant, with appropriate boundary conditions describing the applied bias. A coarse-grained 3D charge density,  $\rho$ , is defined on a grid, projecting the charges within each voxel onto the eight voxel vertices before solving Equation 4. Each hopping site's electrostatic potential then comes from mapping  $\phi$  onto that site. The charge density distribution and potential profile is recalculated after every KMC event.

The use of kinetic Monte Carlo (KMC) models to describe charge transport in OSCs is well established [14–16] and flexible enough to incorporate several levels of detail. A KMC simulation is essentially a Markov chain that consists of a series of discrete events, each with its own waiting time, during which the state of the system does not change. For charge transport in OSCs, this is equivalent to a series of hopping events between sites that are fixed in space. This can be mapped onto a network transport model; each individual hopping site becomes a node in a network; network connections (edges) exist between pairs of sites that a particle can move between in a single



event. The details of the explicit numerical simulation determine the number, range and weighting of the edges between nodes. By using this mapping one can directly compare the results of different KMC models, as well as quantify the nature of transport on a microscopic level.

As mentioned above, this approach requires the calculation of bespoke parameters,  $\Delta G_{ij}$ , for distinct pairs  $ij$ . We calculated the transfer integrals and the site energies using VOTCA-CTP [17–22] with a polarisable Thole model [23]. VOTCA [20] is a toolkit for a variety of molecular coarse-graining applications; VOTCA-CTP builds upon this by calculating the charge transport properties of coarse-grained systems; in this case, we are calculating the orbital overlap not between atoms but between molecules. The electronic orbital information of isolated molecules, the ground states and both ionised states, necessary for VOTCA was calculated using Gaussian [24]. We calculated transfer integrals for all pairs that satisfied the constraint  $r_{ij} < 2.5$  nm, where  $r_{ij}$  is the centre of mass distance between sites  $i$  and  $j$ . This cut-off was chosen as the magnitude of  $J_{ij}^2$  decays exponentially and beyond 2.5 nm; they become sufficiently small while still including non-nearest neighbours (see Figure 4). The probability of charge transfer events occurring over more than 2.5 nm is so small that including these events would not affect the observed charge transport. The electrostatic contributions to  $\Delta G_{ij}$  are calculated using the cloud-in-cell particle-mesh method described by Hockney & Eastwood [13]. We refer to a set of hopping site positions, the associated energies and coupling parameters as a morphology.

The first reaction method (FRM) was used to select the next event to be performed in the KMC simulation [25]. In brief, the FRM method requires us to calculate the rate ( $\nu_k$ ) of every possible event in the system, then for each event draw a waiting time ( $t_w^{(k)}$ ) from a Poissonian distribution parameterised by  $\nu_k$ . At each KMC step we perform the event with the shortest waiting time. We note that given a set of  $M$  events with rates  $\nu_1; \dots; \nu_M$  and waiting times  $t_w^{(1)}; \dots; t_w^{(M)}$ , the probability that the  $k$ th event is performed is given by  $P \propto \nu_k / \sum_{i=1}^M \nu_i$ , which is equivalent to:

$$P(k) = \frac{\nu_k}{\sum_{i=1}^M \nu_i} \quad (5)$$

We ran six simulations with different random number seeds for each morphology. The simulations were initiated with no charge carriers present in the cell. As the simulation ran, injection of charge carriers

took place at the top electrode and extraction at the bottom electrode. Injection was treated as a single step process in which the rate of a carrier being injected onto a random, vacant hopping site adjacent to the electrode is calculated as the Marcus hopping rate from the electrode site to the site in the bulk of the device. The difference in energy is considered as  $\Delta G_{ij} = \frac{q}{4\pi\epsilon_0} \frac{\delta E}{r_{ij}} - E_F + \delta\phi + V$ , where  $E_F$  is the Fermi energy of the electrode,  $V$  is the voltage applied to the electrode and  $ajc$  distinguishes between the anode or cathode.

We note that in any system of discrete, time-sequential reactions, reactions that are slower by orders of magnitude are the rate-determining processes for the total system trajectory. As such, given that the transfer integrals span many orders, the slowest hops are the most important with respect to the macroscopic transport properties. This means we need to capture the full distribution of reactions, including the tail of slow reactions, and use a numerical algorithm that allows slow events to occur. To include all possible events and rates it is important to model large system sizes that will feature many of the pairwise arrangements that are possible at a given statepoint.

Once the dynamics reached steady state with respect to charge injection and extraction, measurements of the mean square displacement,  $\langle \delta r^2 \rangle$ , were taken at intervals of  $\Delta t = 5 \times 10^{-3}$  ps. If  $\Delta t$  is too short, compared to the carrier transit time,  $\langle \delta r^2 \rangle$  is dominated by charge transfer back and forth within a strongly coupled pair, in a rattling motion. To measure the charge carrier motion, we calculated the mean square distance displacement of free charge carriers as a function of time  $\tau$ ,

$$\langle \delta r^2 \rangle = \frac{1}{M} \sum_{i=0}^{M-1} \langle r_i^2 \rangle - \langle r_0^2 \rangle \quad (6)$$

where  $M$  is the number of time steps. The maximum simulation time  $\tau_{\max}$  was set at  $10^8$  ps. Continuous measurements, such as the mean squared displacement (MSD), were averaged over all KMC trajectories. The mobility was measured using:

$$\mu = \frac{D}{k_B T}; \quad D = \lim_{\tau \rightarrow 1} \frac{\langle \delta r^2 \rangle}{\tau} \quad (7)$$

where  $k_B$  is the Boltzmann constant.

## 2.1. Network analysis

To investigate the role of a given pair of molecules in charge transport, as compared to properties of the entire system, we need to use a description that treats

pairs, rather than individual molecules as the simplest individual object. To achieve this we used tools from graph theory [26] that explicitly considers the connections between objects as entities in their own right. We mapped the transfer integrals onto a transportation network, called a graph, that consists of nodes linked by edges; an example is illustrated in Figure 2. In this case, nodes are the HOTT molecules and edges are links between a molecule and all other molecules within the transfer cut-off  $r_c$ .

Network analysis has been used to study organic charge transport networks and kinetic Monte methods before. Jackson et al. used dynamic network techniques to study how the charge transport network changes over time as the molecules move [27]; however, they did not model the resultant charge transport properties. Cottaar et al. used percolation theory on a 2D lattice to describe the effects of correlated and uncorrelated energetic disorder [28]; they considered the percolative pathways in terms of the current density between lattice sites forming edges. The above study was lattice-based and although they showed the existence of favoured charge pathways, they could not relate this to any structural properties of the system and the energetic disorder was drawn from a chosen distribution. Graph theoretical approaches were also applied to KMC simulations of chemical kinetics by Stamatakis & Vlachos [29]; this is still a system of discrete events and the underlying algorithm is similar.

To probe charge transport, we use the charge trajectories to find the elements of a traffic matrix  $T$ , an order  $N$  square matrix with rows and columns each linked to molecules  $i = 1$  to  $N$ . Its diagonal elements are zero. Its off diagonal elements  $T_{ij}$ , are equal to the number of charges that hopped between site  $i$  and site  $j$ , i.e. the traffic from site  $i$  to  $j$ .

We also define the linked traffic,  $\uparrow_{ij}$ , of an edge as the average traffic of the set of neighbouring edges in a

given direction. For an edge from  $i$  to  $j$  this set includes all edges that end at  $i$  or start from  $j$ , excluding the reverse edge from  $j$  to  $i$ . We can write  $\uparrow_{ij}$ :

$$\uparrow_{ij} = \frac{1}{2} \left( \frac{\sum_h T_{hi}}{M_i - 1} + \frac{\sum_k T_{jk}}{M_j - 1} \right) \quad (8)$$

where  $M$  ( $M_j$ ) is the number of neighbouring nodes to node  $i$  ( $j$ ) and  $h$  ( $k$ ) is an index over this set. The sums are over neighbouring edges, so the first (second) sum on the right-hand side is over all edges that begin at site  $i$  ( $j$ ) and end at site  $j$  ( $i$ ). Given that the traffic  $T_{ij}$  is an extensive measurement in time, all traffic measurements are made for the same simulation time  $\tau_{\max}$ . There is a net flux from site  $i$  to  $j$ :

$$F_{ij} = \uparrow_{ij} - \uparrow_{ji} \quad (9)$$

where  $\mathbf{e}_{ij}$  is the unit vector linking sites  $i$  and  $j$ . Note that the flux matrix is skew symmetric.

### 3. Results

We have investigated the charge transport properties of the two morphologies with a focus on exploiting the microscopic resolution given by the self-consistently generated atomistic morphology. Figure 3 shows the generated morphologies in their entirety: the columnar ordering spans the entire system at  $T = 280$  K, with a well described separation between columns. The 400 K morphology is amorphous and the molecules have an isotropic orientation. The  $T = 280$  K system consists of 9011 molecules in a system of size  $15.67 \times 15.67 \times 52.85$  nm. The  $T = 400$  K system size consists of 8968 molecules in a system of size  $16.32 \times 16.32 \times 65.36$  nm.

To investigate the topology of the transport network, completely apart from transport and carriers, we can consider the transfer integrals. They are a static

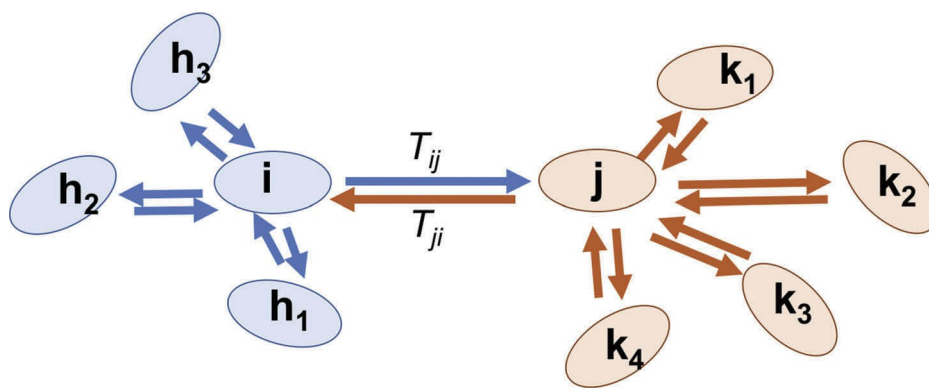
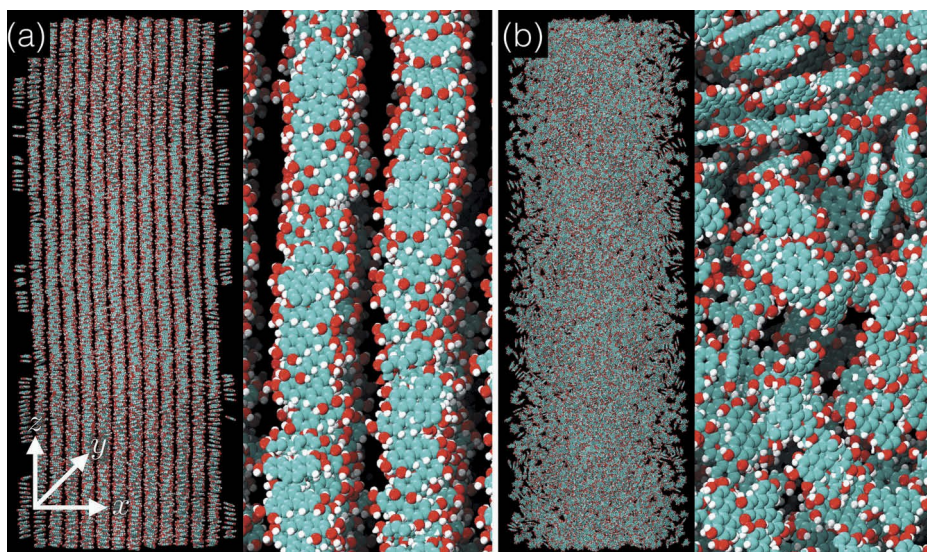


Figure 2. (Colour online) Schematic illustration of the network. Nodes are the molecules shown as ellipses. For each pair of molecules separated by less than  $r_c$ , there are two edges whose directions are shown by the arrows joining the nodes. The node labels show how the linked traffic  $\uparrow_{ij}$  is calculated from Equation 8.



**Figure 3.** (Colour online) A figure showing the complete morphologies. (a) The morphology at  $T = 280\text{K}$ , the long-range columnar order is clear and the close-up shows the extent of local alignment within a column. (b) The morphology at  $T = 400\text{K}$ , there is no long-range order in the system, while the close-up shows that there are some short-range orientational correlations where a few molecules co-align.

property of the network, pertaining to connections between nodes and are not affected by the movement of charges. Figure 4 shows the value of transfer integrals for each pair against the Cartesian components of the pair separation. In terms of the hopping network, the transfer integral between two sites is equal to the weight of the edge between them. The larger the transfer integral, the more strongly connected the two corresponding sites are.

Figure 4(a) shows the edge weights against separation in the columnar morphology; there is a clear structure to the distribution. In the  $x$  and  $y$  components there is a single cluster of highly connected edges ( $J_{ij} > 10^{12}$  eV) around  $\Delta r_{xy} \approx 0$  with a second continuous distribution of edges with ( $J_{ij} < 10^{12}$ ). These edges are intra-column connections; the axial radius of HOTT is  $r_k \approx 0.653$  nm so within  $2r_k$  the sites cannot overlap in the  $xy$  plane. The most strongly connected sites are nearest neighbours in the same column, weaker edges are further neighbours, there are distinct grouping for the second and third nearest neighbours. At distances greater than  $2r_k$ , the edges must correspond to inter-column couplings considering the direction of effective coupling is normal to the axial symmetry of the molecule one would expect this coupling to be relatively weak.

We now consider the strength of transfer integrals against the separation in  $z$ , the right-hand panel of Figure 4(a); there is again a distinction between inter- and intra-column couplings. The dashed line indicates an exponential decay with separation the clusters that

lie along this trend have separations that correlate with intra-column couplings and the radial height of HOTT is  $r_z \approx 0.172$  nm. Recalling that  $J_{ij} \propto \Delta x^2 + \Delta y^2 + \Delta z^2$ , we can associate the two strongest sets of couplings with nearest and second-nearest neighbours within a column. The spacings are close to 0 in the  $xy$  plane and around  $2r_z$  and  $4r_z$  in the  $z$  direction.

The couplings in the amorphous system are identically distributed in the  $xy$  plane and in the  $z$  direction; see Figure 4(b). The distributions are isotropic with no defined structure beyond a slight inflection in the outer edge around  $\Delta r \approx 1$  nm. The strength of these transfer integrals is consistent with nearest neighbour, co-facial couplings. In turn, the pair separations also fit this kind of arrangement, although not aligned to any specific Cartesian axis. This suggests that coupling in the amorphous system is isotropic with an exponential dependence on separation, with a secondary short-range increase in couplings due to molecules with their central aromatic sections parallel.

To quantify charge transport on the scale of the entire system, we measured the MSD, shown in Figure 5, according to Equation 6. The columnar morphology exhibits an order of magnitude faster charge transport, compared to the amorphous system. The MSD does not illustrate why this is; it is simply a measurement of distance travelled, although we can glean some insight by looking at the different Cartesian components. The component of the MSD parallel to a given vector  $\vec{d}$  can be written as



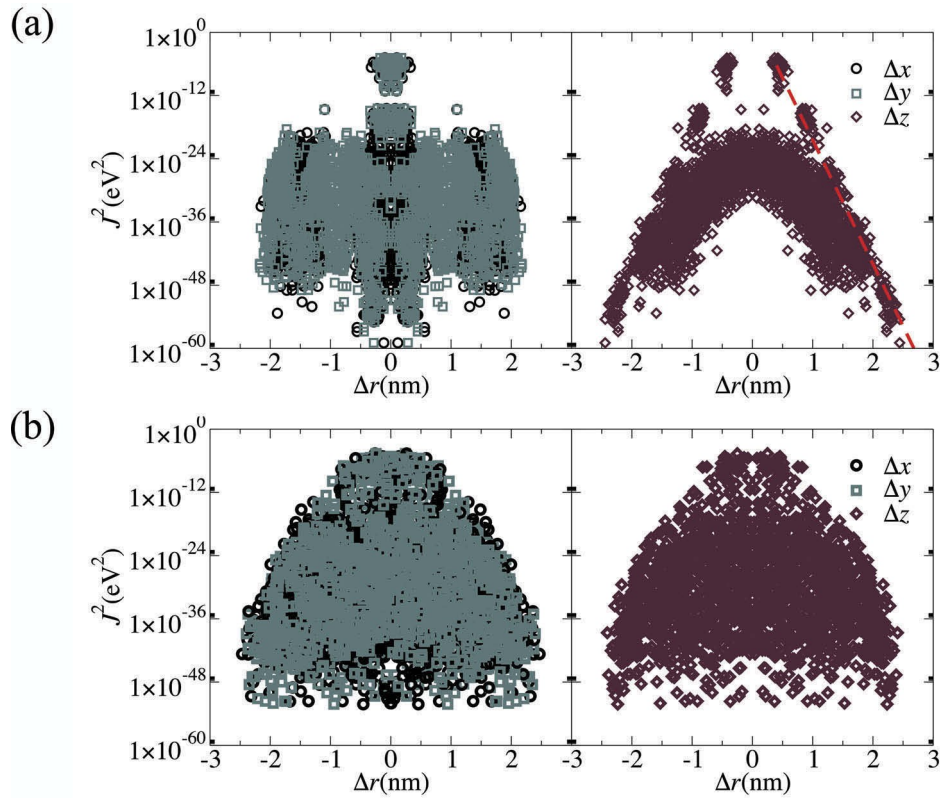


**Figure 4.** (Colour online) The strength of the electronic coupling between hopping sites against the separation between them, divided into Cartesian components. (a) The couplings in the columnar ( $T = 280\text{K}$ ) system: these show a clear spatial structure and we can relate transport properties explicitly to the molecular structure. (b) The couplings in the amorphous ( $T = 400\text{K}$ ) system: there is no structure to the couplings beyond an exponential decay with increasing separation, the transport properties are isotropic.

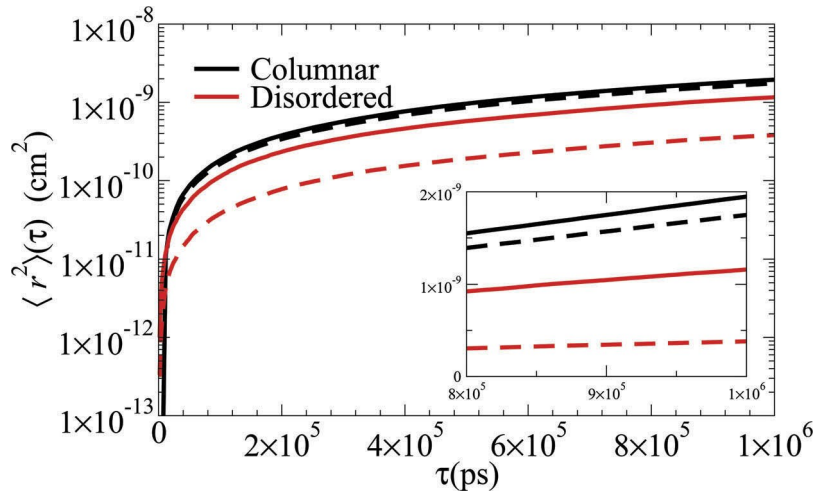


**Figure 5.** (Colour online) The MSD measured in the two morphologies in the dimensions (solid lines) and parallel to the z axis (dashed lines) at an applied bias of 2.0V. The charge transport is an order of magnitude slower in the disordered system, although this does not provide any information about the nature of the transport nor why it is slower. More tellingly the z component of the MSD is roughly equal to one third of the total MSD in the amorphous system while they are roughly equal in the ordered structure.

$$h_{d0}^2 \delta \tau_{Bi} \frac{1}{N} \sum_{j=0}^M \frac{1}{N} \sum_{i=0}^N \langle \mathbf{r}_i \cdot \mathbf{r}_j \rangle \propto \Delta t \propto \tau_{ij} \propto \frac{1}{\delta} \propto \frac{1}{\delta^2} \propto \frac{1}{\delta^3}$$

In a 3D system with isotropic transport then  $h_{d0}^2 \propto h_{d0}^2$  for any two vectors  $\mathbf{d}$  and  $\mathbf{d}'$ , and  $h_{d0}^2 \propto \frac{1}{3} h_{d0}^2$ . We measured the component of the MSD parallel to the z axis, the same direction as the column axis and the applied field, shown as the dashed lines in Figure 5.

In the amorphous system, this is indeed equal to one third of the total MSD, indicating that the transport is isotropic. However, there is an applied field in the z-direction that should drive charge transport. From measuring the MSD it seems that the field has little effect on the axis of transport, although it may have an effect on the net direction of transport (the MSD does not distinguish between 'forward' and 'backward' movement).

In comparison, the columnar system is very different, meaning that most of the carrier motion is parallel to the column axis. The presence of directional transfer in columnar discotics was also predicted by Bacchiocchi & Zannoni using a simplified Monte Carlo model [10]. Thus we can state that the transport in the amorphous system is isotropic while in the ordered columnar system it is highly directed and responds to an applied

field. In the context of a full-scale device, this is equivalent to a state which can be switched 'on' and 'off' with an external voltage. In both cases the transport reflects the topology of the system and more importantly, the underlying transport network.

The MSD is a rather coarse measure of transport across the system on long length and timescales. With the detailed, equilibrium molecular morphology provided by the CGMD it would be a shame not to investigate transport on a microscopic scale. We recorded the traffic and flux between all hopping sites during a simulation and plotted the resulting network properties in Figure 6. We show the electronic couplings, the traffic and the flux between molecules in space. The figures showing the traffic (Figure 6 (c-d)) reveal the short-range nature of the hops; this is expected from the distribution of  $|J_{ij}|^2$ .

The ratio of traffic to flux is the most striking result of the network analysis. The traffic along an edge can range up to  $10^5$  hops, while the total flux has a maximum of 3 hops during a simulation (see Figure 6(c-f)). A study of coarse-grained transports such as a drift-diffusion model or the extended Gaussian disorder model, would not be able to resolve the extent of this back and forward 'rattling' motion. Quantifying the

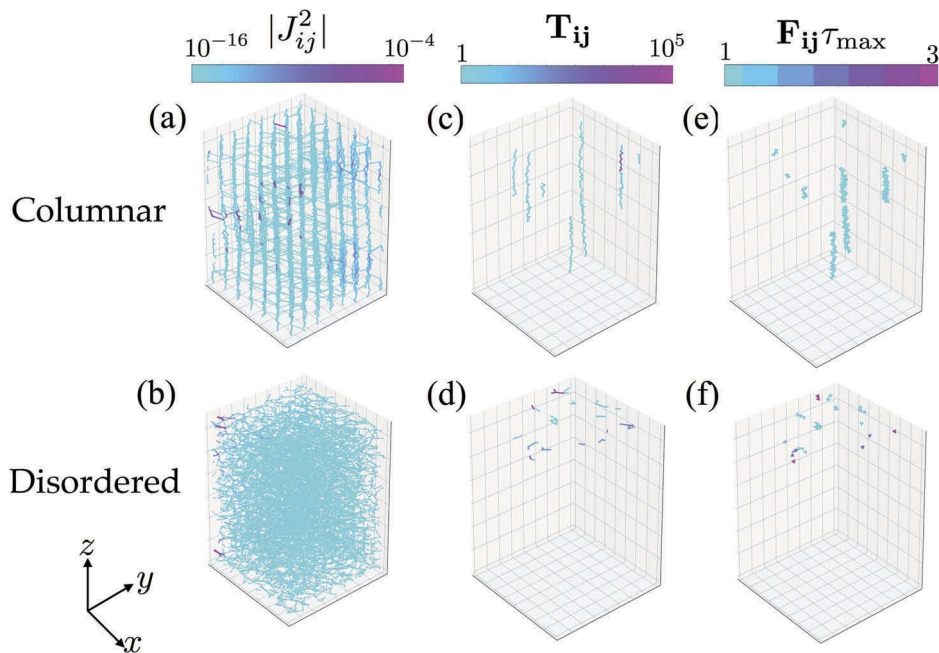


**Figure 6.** (Colouronline) Figures showing the microscopic transport behaviour in the two HOTT systems. (a, b) The spatial distribution of the electronic coupling in the molecular structure is clear (compared to Figure 4). Note the relative dearth of inter-column couplings in (a). (c, d) The traffic between sites as defined in Section 2. The traffic is confined within a column in the 280 K system, effectively resulting in filamentary one-dimensional transport. In the amorphous 400 K system the traffic occurs in isolated pockets with carriers moving between a small number of sites. (e, f) The time integrated flux in the two systems is equal to the total flux between sites during the simulation. In the columnar system the flux is necessarily confined to columns like the traffic, but with a net direction (indicated by arrows). In the amorphous system the flux has the same spatial heterogeneity as the traffic. In both systems the flux is of similar magnitude.

extent of rattling in organic systems is an important step forward in charge transport modelling: high levels of fast, local motion can lead to dissipative heating and degradation in the worst case; and as a carrier trap, reducing mobility in all cases. The ability to resolve the motion is key to understanding and preventing it.

As we can see in Figure 6(c-d), the transport is extremely heterogeneous and none of the conducting pathways span the entire system in the simulation time ( $10^8$  ps). That means that a given charge carrier is not being injected and extracted in the time observed, hence there is no flux across the entire system and, in a sense, all motion is rattling on the length scale of  $\sim 50$  nm. Given the number of isolated transport regions, and their difference in size and shape, we study the properties of these pathways.

Each charge carrier visits a set of molecules that form a connected cluster in the system (a subgraph of nodes in the transport network); if two clusters overlap then they combine to form a single larger cluster. The smaller and more isolated the clusters are, the faster the rattling is as the maximum possible length of a closed loop becomes smaller. On the macroscopic scale any cluster that does not span the entire system (percolate the system) will lead to rattling. Figure 7 shows the size distribution of clusters, measured along the z axis, with respect to the number of molecules in the cluster  $N$ .

In the columnar system, the length of the clusters are linearly correlated with  $N$  (see Figure 7), reinforcing their filamentary nature. More importantly, the length of the clusters increases with simulation time and the distribution remains linear with size; thus, the clusters

will eventually percolate the system, unless the column is structurally disrupted. By contrast, the length of clusters in the amorphous system is correlated with  $N^{1/3}$ , suggesting that the clusters are roughly isotropic.

It is known that one-dimensional transport will eventually fail as a single fault will completely disrupt the entire transport network. In the system sizes simulated here, the columns percolate; thus, we cannot describe the effect of dislocations to the charge transport. However, the study of the amorphous system shows that if two columnar regions are separated by a small amorphous region (a 1D crystal defect), transport will still occur, albeit slowly. The regions between columns would effectively transport charge an order of magnitude more slowly than the columns; they would be the limiting factor to the overall performance of the device. The concept that underlying structural heterogeneity causes transport heterogeneity has been discussed in molecular charge transport systems [30]. The relative sizes, arrangement and speeds of the 'fast' and 'slow' regions dictate the net transport and it is key to get all of these correct.

In a more general sense this shows the importance of obtaining sufficient statistics when modelling disordered systems, either by modelling larger systems or several independent systems of the same size. Kordt et al. [31] have calculated the required system sizes to produce accurate charge transport results as a function of energetic disorder. However, they do not consider explicit structural defects. It is known that the columnar phase exhibits defects where the local columnar ordering is disrupted by nematic regions, and the

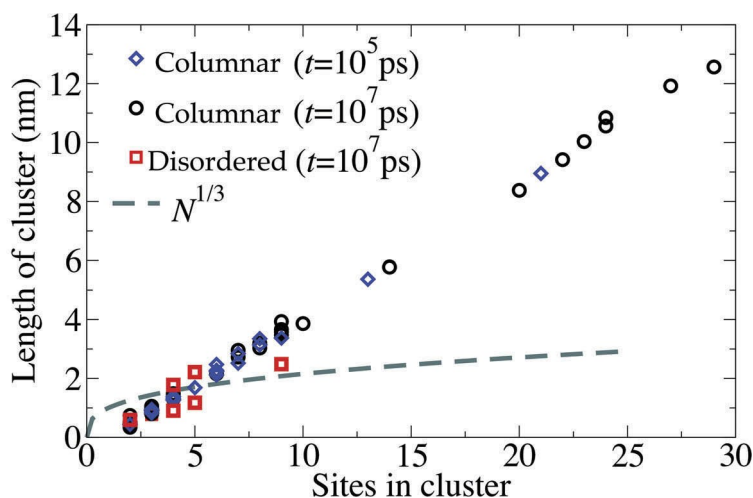


Figure 7. (Colour online) The length of connected clusters of molecules measured parallel to the z axis plotted against the number of molecules in the cluster. The dashed line shows the expected dependence for isotropic clusters. The columnar system clusters are one-dimensional as shown by the linear dependence between length and size. Clusters in the amorphous system are more isotropic and are smaller in terms of the number of sites. The linear clusters grow with time and will eventually percolate the system.

coarse-grained model used in this study can reproduce them [8], although we do not see them in our sample. However, if we simulate a larger system size (or averaged over multiple independent configurations), we would expect to observe defects and thus would be able to model the effect of defects upon transport.

Although this study is not conclusive, we suggest that our ability to describe an entirely isotropic system shows that the methodology presented could accurately predict the charge transport properties around and across defect regions; the CGMD model is accurate enough to reproduce defects at realistic densities and the charge transport parameters are calculated for the specific positions and orientation of molecules. The network terminology we introduce to quantify charge transport properties is also completely general and can be applied to any discrete hopping system. This reduces the issue of large statistical sampling down to one of computational resource, both for morphology generation and transport modelling, a non-trivial concern given the costs of molecular dynamics simulations. Using coarse-grained potentials for molecules is the only feasible method to generate morphologies on the scales required.

To get an estimate of how few edges contribute to charge transport, we can compare  $N_e^0$ , the number of edges where  $T_j > 0$ , to the total number of edges  $N_e$ . At a bias of 2V in the columnar phase, the ratio  $N_e^0/N_e \approx 1:17 \times 10^3$  is an indicator of the variability in transport behaviour between molecules. In the disordered system the ratio is an order of magnitude smaller, carrier hops are more localised along fewer edges. This suggests that the distribution of hopping rates is more sparse.

To quantify the degree of rattling motion we calculate  $N_{\text{hops}} \propto \frac{1}{2} \sum_j |F_{ij}|$ , the number of carrier hops that contribute to a flux. The ratio of  $N_{\text{hops}}$  to the total number of recorded hops is small, of the order  $10^4$  in the columnar phase and an order of magnitude smaller in the disordered phase, suggesting that most carrier hops represent rattling motion. Table 1 shows the precise values for the calculated

three-dimensional charge mobility,  $\mu$ , the mobility parallel to the z axis,  $\mu_z$ , the ratio of contributing edges and the ratio of hops that contribute to flux.

## 4. Conclusions

To accurately describe charge transport in an OSC system requires an accurate description of the structure. The molecular interactions are key to the resultant structure and, crucially, the regions of high electronic overlap. These regions are key to the electronic couplings that form the charge transport network. Without a detailed, atomically resolved structure of the system, one cannot calculate bespoke transfer integrals for each pair of molecules. We have demonstrated a self-consistent methodology that allows us to model the charge transport properties of a molecule without parameterising the transport. All of the necessary quantities to compute hopping rates (see Equation 2) are calculated for each pair of molecules and each possible hop.

The only step which requires parameterisation is the development of the coarse-grained MD potential. The use of Gay-Berne potentials to describe the interactions and structure of liquid crystal molecules, including triphenylenes, is well proven. It is unfeasible to model these systems at the length scales required to describe the structural dependency of inter-molecular charge transport, without the use of coarse-grained molecular models. We have shown that the system sizes and resolution made available by these methods allow accurate description of charge transport in multiple phases.

We have introduced a very general framework, based upon multiscale modelling and network theory descriptions, to describe any discrete charge transport process between molecules. Although we have not applied the method to systems with acute structural changes, i.e. localised structural defects or impurities, we hope to apply the same methodology to these cases in the future.

Using CGMD morphologies we have shown that a system of semiconducting liquid crystal discotics vary their charge mobility by an order of magnitude depending on the large-scale molecular structure. Note that if we had used an isotropic exponential decay to describe the electronic coupling then we would not reproduce these results. Recall Figure 4 where there are many pairs with equally small values of  $t_{ij}$  in both systems; however, the strongest couplings dominate. This illustrates the importance of the specific molecular packing in OSCs and the weakness of using lattice-based or overly parameterised models. We encourage further investigation of the effect of molecule shape and packing with respect to charge transport.

**Table 1.** The precise values of charge transport observables, defined in the main text, from KMC trajectories at  $T = 300\text{K}$  under an applied bias of 2.0V.

	T = 280K	T = 400K
$\mu \text{ cm}^2 \text{ V}^{-1} \text{ s}^{-1} \text{ } \rho$	$1.783 \times 10^{-6}$	$8.757 \times 10^{-7}$
$\mu_z \text{ cm}^2 \text{ V}^{-1} \text{ s}^{-1} \text{ } \rho$	$4.782 \times 10^{-6}$	$7.938 \times 10^{-7}$
$N_e^0/N_e$	$1.49 \times 10^{-3}$	$3.18 \times 10^{-4}$
$N_{\text{hops}}/N_{\text{hops}}$	$1.54 \times 10^{-4}$	$5.3 \times 10^{-5}$



## References

- [1] Groves C. Simulating charge transport in organic semiconductors and devices: a review. *Rep Prog Phys* **2017** Feb;80:026502.
- [2] Mesta M, Carvelli M, De Vries RJ, et al. Molecular-scale simulation of electroluminescence in a multilayer white organic light-emitting diode. *Nat Mater*. **2013**;12:652–658.
- [3] Bäassler H. Charge transport in disordered organic photoconductors: a Monte Carlo simulation study. *Phys Status Solidi B* **1993** Jan;175:15–56.
- [4] Baranovskii SD. Theoretical description of charge transport in disordered organic semiconductors. *Phys Status Solidi B*. **2014** Feb;251:487–525.
- [5] Watkins PK, Walker AB, Verschoor GLB. Dynamical Monte Carlo modelling of organic solar cells: the dependence of internal quantum efficiency on morphology. *Nano Lett*. **2005** Sept;5:1814–1818.
- [6] Papadopoulos TA, Muccioli L, Athanasopoulos S, et al. Does supramolecular ordering influence exciton transport in conjugated systems? Insight from atomistic simulations. *Chem Sci* **2011**;2:1025–1032.
- [7] Nenashev AV, Dvurechenskii AV, Gebhard F, et al. Field dependence of hopping mobility: lattice models against spatial disorder. *Phys Rev B* **2017**;96:1964.
- [8] Orlandi S, Muccioli L, Ricci M, et al. Core charge distribution and self assembly of columnar phases: the case of triphenylenes and azatriphenylenes. *Chem Cent J*. **2007**;1:15–13.
- [9] Lamarra M, Muccioli L, Orlandi S, et al. Temperature dependence of charge mobility in model discotic liquid crystals. *Phys Chem Chem Phys* **2012**;14:5368–8.
- [10] Bacchicocchi C, Zannoni C. Directional energy transfer in columnar liquid crystals: a computer-simulation study. *Phys Rev E* **1998** Aug;58:1–8.
- [11] Emerson AP, J. Luckhurst GR, Whatling SG. Computer simulation studies of anisotropic systems. *Mol Phys*. **2006** Aug;82:113–124.
- [12] Marcus RA. On the theory of oxidation-reduction reactions involving electron transfer. *J Chem Phys*. **1956** May;24:966–978.
- [13] Hockney RW, Eastwood JW. Computer simulation using particles. Bristol, UK: CRC Press; **1988** Jan.
- [14] Groves C, Kimber RGE, Walker AB. Simulation of loss mechanisms in organic solar cells: a description of the mesoscopic Monte Carlo technique and an evaluation of the first reaction method. *J Chem Phys*. **2010** Oct;133:144110.
- [15] Kimber RGE, Wright EN, O'Kane SEJ, et al. Mesoscopic kinetic Monte Carlo modeling of organic photovoltaic device characteristics. *Phys Rev B* **2012**;86:235206.
- [16] Mass´E A, Friederich P, Symalla F, et al. Ab initio charge-carrier mobility model for amorphous molecular semiconductors. *Phys Rev B* **2016**;93:195209.
- [17] Rühle V, Junghans C, Lukyanov A, et al. Versatile object-oriented toolkit for coarse-graining applications. *J Chem Theory Comput* **2009**;5:3211–3223.
- [18] Baumeier B, Kirkpatrick J, Andrienko D. Density-functional based determination of intermolecular charge transfer properties for large-scale morphologies. *Phys Chem Chem Phys* **2010**;12:11103–11113.
- [19] Lukyanov A, Andrienko D. Extracting nondispersive charge carrier mobilities of organic semiconductors from simulations of small systems. *Phys Rev B*. **2010**;82:193202.
- [20] Rühle V, Lukyanov A, May F, et al. Microscopic simulations of charge transport in disordered organic semiconductors. *J Chem Theory Comput*. **2011**;7:3335–3345.
- [21] Kordt P, Andrienko D. Modeling of spatially correlated energetic disorder in organic semiconductors. *J Chem Theory Comput*. **2015** Dec;12:36–40.
- [22] Poelking C, Andrienko D. Long-range embedding of molecular ions and excitations in a polarizable molecular environment. *J Chem Theory Comput*. **2016** Aug;12:4516–4523.
- [23] Van Duijnen PT, Swart M. Molecular and atomic polarizabilities: Thole's model revisited. *J Phys Chem*. **1998** Apr;102:2399–2407.
- [24] Frisch MJ, Schlegel HB, Scuseria GE, et al. Gaussian 09 revision A.02. **2009**.
- [25] Gillespie DT. A general method for numerically simulating the stochastic time evolution of coupled chemical reactions. *J Comp Phys*. **1976** Dec;22:403–434.
- [26] Wilson RJ. Introduction to graph theory. Longman Scientific and Technical; Upper Saddle River, NJ: Longman. **1985**.
- [27] Jackson NE, Chen LX, Ratner MA. Charge transport network dynamics in molecular aggregates. *PNAS*. **2016** Aug;113:8595–8600.
- [28] Cottaar J, Coehoorn R, Bobbert PA. Scaling theory for percolative charge transport in molecular semiconductors: correlated versus uncorrelated energetic disorder. *Phys Rev B* **2012** June;85:877.
- [29] Stamatakis M, Vlachos DG. A graph theoretical kinetic Monte Carlo framework for on-lattice chemical kinetics. *J Chem Phys* **2011** June;134:214115.
- [30] Noriega R, Rivnay J, Vandewal K, et al. A general relationship between disorder, aggregation and charge transport in conjugated polymers. *Nat Mater*. **2013**;12:1038–1044.
- [31] Kordt P, Speck T, Andrienko D. Finite size scaling of charge carrier mobility in disordered organic semiconductors. *Phys Rev B* **2016** July;94:014208.